χ-Conotoxin and Tricyclic Antidepressant Interactions at the Norepinephrine Transporter Define a New Transporter Model

Filip A. Paczkowski, Iain A. Sharpe, Sébastien Dutertre, Richard J. Lewis

Membrane Transport, Structure, Function, and Biogenesis:

δ-Conotoxin and Tricyclic Antidepressant Interactions at the Norepinephrine Transporter Define a New Transporter Model

Filip A. Paczkowski, Iain A. Sharpe, Sébastien Dutertre and Richard J. Lewis

J. Biol. Chem. 2007, 282:17837-17844.
doi: 10.1074/jbc.M610813200 originally published online April 11, 2007

THE JOURNAL OF BIOLOGICAL CHEMISTRY VOL. 282, NO. 24, pp. 17837–17844, June 15, 2007

χ-Conotoxin and Tricyclic Antidepressant Interactions at the Norepinephrine Transporter Define a New Transporter Model*

Received for publication, November 22, 2006, and in revised form, March 26, 2007 Published, JBC Papers in Press, April 11, 2007, DOI 10.1074/jbc.M610813200

Filip A. Paczkowski, Iain A. Sharpe, Sébastien Dutertre[1], and Richard J. Lewis[2]

From the Institute for Molecular Bioscience, The University of Queensland, Brisbane, Queensland 4072, Australia

Monoamine neurotransmitter transporters for norepinephrine (NE), dopamine and serotonin are important targets for antidepressants and analgesics. The conopeptide χ-MrIA is a noncompetitive and highly selective inhibitor of the NE transporter (NET) and is being developed as a novel intrathecal analgesic. We used site-directed mutagenesis to generate a suite of mutated transporters to identify two amino acids (Leu^{469} and Glu^{382}) that affected the affinity of χ-MrIA to inhibit [^{3}H]NE uptake through human NET. Residues that increased the K_d of a tricyclic antidepressant (nisoxetine) were also identified (Phe^{207}, Ser^{225}, His^{296}, Thr^{381}, and Asp^{473}). Phe^{207}, Ser^{225}, His^{296}, and Thr^{381} also affected the rate of NE transport without affecting NE K_m. In a new model of NET constructed from the bLeuT crystal structure, χ-MrIA-interacting residues were located at the mouth of the transporter near residues affecting the binding of small molecule inhibitors.

The monoamine neurotransmitter transporters are part of a larger family of Na^+- and Cl^--dependent transporters found in bacteria through to mammals. Dopamine, serotonin, and norepinephrine transporters (DAT,[3] SERT and NET, respectively) mediate the neuronal reuptake of their cognate neurotransmitter substance, terminating neurotransmission. NET has been implicated in mood states including depression and arousal, as well as in the control of blood pressure and pain (1–5), and is one of the targets of many psychoactive compounds including stimulants and antidepressants. Precisely how these compounds bind to NET is not well understood, but their interactions appear distinct from those of norepinephrine (NE) (6–9). Unlike NE, tricyclic antidepressants such as desipramine and nisoxetine are not transported and appear to block by occluding the pore of the transporter.

χ-MrIA is a peptide isolated from the venom of the predatory marine snail *Conus mamoreus* (10). This conopeptide specifically inhibits NE transport by NET without affecting dopamine or serotonin uptake by DAT and SERT, respectively (10, 11) and suppresses neuropathic pain upon intrathecal administration to rodents (5). χ-MrIA is a non-competitive inhibitor of NE transport but a competitive inhibitor of tricyclic antidepressants binding (11). Since desipramine and nisoxetine competitively inhibit NE transport, it appears that the binding site of χ-MrIA overlaps the antidepressant but not the NE binding site.

There is currently no crystal structure of NET. Hence, structural details have been inferred from hydrophobicity, site-directed mutagenesis (performed mostly on related DAT and SERT proteins), and sequence analysis and subsequent computer homology models based on related bacterial transporters (12–19). NET and other monoamine neurotransmitter transporters are predicted to have 12 membrane-spanning regions, intracellular C and N termini, and a large extracellular loop between transmembrane domains 3 and 4. A more detailed view of monoamine transporters is starting to emerge with the recent crystal structure of a bacterial leucine transporter (bLeuT) (20), the closest functionally related transporter crystallized to date. Like monoamine transporters, bLeuT is Na^+-dependent with 12 membrane-spanning regions. bLeuT shares 28% identity with human NET (hNET) (see Fig. 1).

In the present study, we used a combination of site-directed mutagenesis and homology modeling to locate residues on the hNET that interact with χ-MrIA. In the process, we identified a number of new interactions that affect NE transport and small molecule antidepressant binding at hNET. These results support a new model of NET constructed from the bacterial leucine transporter crystal structure.

EXPERIMENTAL PROCEDURES

Materials—Desipramine hydrochloride, dopamine hydrochloride, nisoxetine hydrochloride and (−)-norepinephrine bitartrate were obtained from Sigma. U-0521 and GBR-12909 dihydrochloride were from Biomol (Plymouth Meeting, PA). *levo*-[*ring*-2,5,6-^{3}H]Norepinephrine (specific activity: 57.9 Ci/mmol), [*N-methyl*-^{3}H]nisoxetine hydrochloride (specific activity: 85.0 Ci/mmol), and 3,4[*ring*-2,5,6-^{3}H]dihydroxyphenylethylamine (dopamine) (specific activity: 60 Ci/mmol) was obtained from PerkinElmer Life Sciences.

Site-directed Mutagenesis—The QuikChange site-directed mutagenesis kit (Stratagene, La Jolla, CA) was used with the human NET to produce mutant cDNAs. Oligonucleotide primers were designed and obtained as custom syntheses (Proligo

* This work was supported by National Health and Medical Research Council Program and Project Grants. The costs of publication of this article were defrayed in part by the payment of page charges. This article must therefore be hereby marked "*advertisement*" in accordance with 18 U.S.C. Section 1734 solely to indicate this fact.

[1] Recipient of a University of Queensland Postgraduate Scholarship.

[2] To whom correspondence should be addressed: Institute for Molecular Bioscience (QBP), The University of Queensland, St. Lucia, 4072, Qld, Australia. Tel.: 617-3346-2984; Fax: 617-3346-2101; E-mail: r.lewis@imb.uq.edu.au.

[3] The abbreviations used are: DAT, dopamine transporter; NE, norepinephrine; NET, norepinephrine transporter; hNET, human NET; SERT, serotonin transporter; DMI, desipramine; bLeuT, bacterial leucine transporter; TM, transmembrane.

A

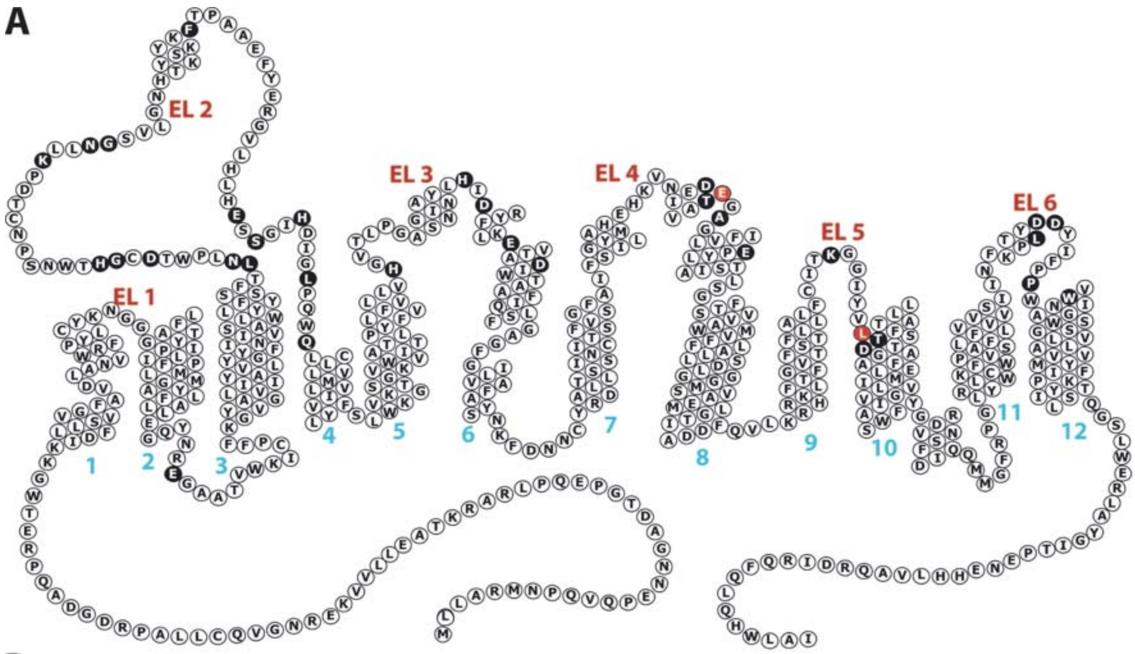

B

```
hNET     1  MLLARMNPQVQPENNGADTGPEQPLRARKTAELLVVKERNG-VQC----LLAPRDG------------------DAQPRE
hDAT     1  --MSKSKCSVGLMSSVVAPAKEPNAVGPKEVELILVKEQNG-VQLTSSTLTNPRQSP-----------------VEAQDRE
hSERT    1  METTPLNSQKQLSACEDGEDCQENGVLQKVVPTPGDKVESGQISNGYSAVPSPGAGDDTRHSIPATTTTLVAELHQGERE
bLeuT    1  ---------------------------------------------------------------------------MEVKRE

              TM1a        TM1b             TM2
hNET    58  TWGKKIDFLLSVVGFAVDLANVWRFPYLCYKNGGGAFLIPYTLFLIIAGMPLFYMELALGQYNREGAATVWK-ICP----
hDAT    61  TWGKKIDFLLSVIGFAVDLANVWRFPYLCYKNGGGAFLVPYLLFMVIAGMPLFYMELALGQFNREGAAGVWK-ICP----
hSERT   81  TWGKKVDFLLSVIGYAVDLGNVWRFPYICYQNGGGAFLLPYTIMAIFGGIPLFYMELALGQYHRNGCISIWRKICP----
bLeuT    7  HWATRLGLILAMAGNAVGLGNFLRFPVQAAENGGGAFMIPYIIAFLLVGIPLMWIEWAMGRYGGAQGHGTTPAIFYLLWR

              TM3
hNET   132  --FFKGVGYAVILIALYVGFYYNVIIAWSLYYLFSSFTLNLPWTDCGHTWNSPNCTDPKLLNGSVLGNHTKYSKYKFTPA
hDAT   136  --ILKGVGFTVILISLYVGFFYNVIIAWALHYLFSSFTTELPWIHCNNSWNSPNCSDAHPGD-SSGDSSGLNDTFGTTPA
hSERT  158  --IFKGIGYAICIIAFYIASYYNTIMAWALYYLISSFTDQLPWTSCKNSWNTGNCTNYFSED------NITWTLHSTSPA
bLeuT   87  NRFAKILGVFGLWIPLVVAIYYVYIESWTLGFAIKFLVGLVPEP-------PPNAT---------------DPDSILRPF

                                 TM4                        TM5
hNET   210  AEFYERGVLHLHESSGIHDIGLPQWQLLLCLMVVVIVLYFSLWKGVKT-SGKVVWITATLPYFVLFVLLVHGVTL--P--
hDAT   213  AEYFERGVLHLHQSHGIDDLGPPRWQLTACLVLVIVLLYFSLWKGVKT-SGKVVWITATMPYVVLTALLLRGVTL--P--
hSERT  230  EEFYTRHVLQIHRSKGLQDLGGISWQLALCIMLIFTVIYFSIWKGVKT-SGKVVWVTATFPYIILSVLLVRGATL--P--
bLeuT  145  KEFLYSYIGVPKG---DEPILKPSLFAYIVFLITMFINVSILIRGISKGIERFAKIAMPTLFILAVFLVIRVFLLETPNG

                          TM6a             TM6b                  TM7
hNET   285  GASNGINAYLHIDFYRLKEATVWIDAATQIFFSLGAGFGVLIAFASYNKFDNNCYRDALLTSSINCITSFVSGFAIFSIL
hDAT   288  GAIDGIRAYLSVDFYRLCEASVWIDAATQVCFSLGVGFGVLIAFSSYNKFTNNCYRDAIVTTSINSLTSFSSGFVVFSFL
hSERT  305  GAWRGVLFYLKPNWQKLLETGVWIDAAAQIFFSLGPGFGVLLAFASYNKFNNNCYQDALVTSVVNCMTSFVSGFVIFTVL
bLeuT  222  TAADGLNFLWTPDFEKLKDPGVWIAAVGQIFFTLSLGFGAIITYASYVRKDQDIVLSGLTAATLNEKAEVILGGSISIPA

                                                         TM8
hNET   365  GYMA--HEHKVNIEDVAT-EGAGLVFILYPEAISTLSGSTFWAVVFFVMLLALGLDSSMGGMEAVITGLADDFQVLKR-H
hDAT   368  GYMA--QKHSVPIGDVAK-DGPGLIFIIYPEAIATLPLSSAWAVVFFIMLLTLGIDSAMGGMESVITGLIDEFQLLHR-H
hSERT  385  GYMA--EMRNEDVSEVAKDAGPSLLFITYAEAIANMPASTFFAIIFFLMLITLGLDSTFAGLEGVITAVLDEFPHVWAKR
bLeuT  302  AVAFFGVANAVAIAKAG---AFNLGFITLPAIFSQTAGGTFLGFLWFFLLFFAGLTSSIAIMQPMIAFLEDELKL----S

              TM9                         TM10
hNET   441  RKLFTFGVTFSTFLLALFCITKGGIYVLTLLDTFAAGTSILFAVLMEAIGVSWFYGVDRFSNDIQQMMGFRPGLYWRLCW
hDAT   444  RELFTLFIVLATFLLSLFCVTNGGIYVFTLLDHFAAGTSILFGVLIEAIGVAWFYGVGQFSDDIQQMTGQRPSLYWRLCW
hSERT  461  RERFVLAVVITCFFGSLVTLTFGGAYVVKLLEEYATGPAVLTVALIEAVAVSWFYGITQFCRDVKEMLGFSPGWFWRICW
bLeuT  375  RKHAVLWTAAIVFFSAHLVMFL--NKSLDEMDFWAGTIGVVFFGLTELIIFFWIFGADKAWEEINRGGIIKVPRIYYYVM

              TM11                    TM12
hNET   522  KFVSPAFLLFVVVVSIINFKPLTYDDYIFPPWANWVGWGIALSSMVLVPIYVIYKFLSTQGSLWERLAYGITPENEHHLV
hDAT   525  KLVSPCFLLFVVVVSIVTFRPPHYGAYIFPDWANALGWVIATSSMAMVPIYAAYKFCSLPGSFREKLAYAIAPEKDRELV
hSERT  542  VAISPLFLLFIICSFLMSPPQLRLFQYNYPYWSIILGYCIGTSSFICIPTYIAYRLIITPGTFKERIIKSITPETPTEIP
bLeuT  453  RYITPAFLAVLLVVWAREYIPKIMEETH---WTVWITRFYIIGLFLFLTFLVFLAERRRNHESA----------------

hNET   602  AQRDIRQFQLQHWLAI
hDAT   605  DRGEVRQFTLRHWLKV
hSERT  622  -CGDIRLNAV------
```

Australia Pty. Ltd., Lismore, Australia). Custom primers of human NET were used to create the point mutants E122A, L169T, N170E, D175A, G177N, H178N, K189H, N192D, G193S, F207T, E223Q, S225H, H228D, L232P, Q234R, H296S, D298A, E304A, D310A, D378A, T381K, E382A, A384P, E393A, K463N, L469A, L469F, D473A, T474H, L543P, D546G, D547A, P552D and W556A, and the double mutants L114S + L469F, L232P + L469F, and L469F + L543P. F472L of the human DAT was also produced. A DAT loop 2 chimera was constructed by using restriction sites for XhoI and SacII present in the large extracellular loop of NET. The appropriate sequence of DAT loop 2 was ligated into the NET (NET residues 166–210) and site directed mutagenesis (Stratagene) was used to reorient a frameshift that occurred during the ligation process. Sequencing was used to determine the correct orientation of the EL2 chimera. *Escherichia coli* were transformed with mutant cDNA and subsequently used for plasmid preparation using a Wizard SV plasmid preparation kit (Beckman Coulter Australia Pty. Ltd., Gladesville, Australia) or a Qiagen mini preparation kit (Qiagen Pty. Ltd., Doncaster, Australia). Samples of purified mutant cDNA were prepared for automatic sequencing using a Big-Dye Terminator kit (Applied Biosystems, Melbourne, Australia), with custom synthesized sequencing primers (Invitrogen or Sigma-Aldrich) and the cDNA from plasmid preparations. Samples were sent to the Australian Genome Research Facility (University of Queensland, Queensland, Australia) for automated sequencing to confirm each mutation.

Cellular Uptake of [^{3}H]Norepinephrine, [^{3}H]Dopamine, and Binding of [^{3}H]Nisoxetine—Cellular accumulation of NE, dopamine, and determination of inhibitor IC_{50} values were performed in 24-well plates as described previously (11) or for norepinephrine uptake and nisoxetine binding assays in a modified 96-well plate assay. Briefly, COS-1 cells (ATCC; Manassas, VA) were grown in 96-well plates (Nunclon; Nalge Nunc International, Rochester, NY) containing Dulbecco's modified Eagle's medium (Invitrogen) and 10% fetal bovine serum (Invitrogen) at 37 °C in 5% CO_2. The cells were transiently transfected with purified plasmid DNA encoding the human NET (hNET) (12) or mutant NETs using Metafectene reagent (Biontex Laboratories GmbH, Munich, Germany). Assays measuring uptake were performed 48 h after transfection at room temperature. The culture medium was removed and the cells were gently washed three times with 150 μl of transport buffer containing 125 mM NaCl, 4.8 mM KCl, 1.2 mM $MgSO_4$, 1.2 mM KH_2PO_4, 1.3 mM $CaCl_2$, 25 mM HEPES, 5.55 mM D-(+)-glucose, 1.0 mM ascorbic acid, 0.1% bovine serum albumin, 10 μM U-0521 (to inhibit catechol-*O*-methyltransferase) and 100 μM pargyline (to inhibit monoamine oxidase) at pH 7.4. The final reaction volume was 50 μl. Nonspecific uptake of [^{3}H]NE by transfected cells was defined by the accumulation occurring in the presence of 100 μM desipramine or 100 μM nisoxetine. Transfected cells were exposed to [^{3}H]NE for 5–8 min at room temperature. The solution containing free [^{3}H]NE was then rapidly removed, and the cells washed three times with 200 μl of ice-cold transport buffer without bovine serum albumin. The cells were lysed with 50 μl 0.1 M NaOH at room temperature with gentle shaking. 30 μl of the cell lysate was used to determine the level of radioactivity by liquid scintillation counting and the remaining 20 μl was used for protein determination. Triplicate measures were made for each experiment ($n = 3–8$ experiments). Specific uptake of [^{3}H]NE was defined as the difference between total uptake and that occurring in the presence of 100 μM desipramine or 100 μM nisoxetine.

Assays measuring [^{3}H]nisoxetine binding were performed 48 h after transfection on whole cells. Cells were trypsinized from standard plasticware and counted using a hemocytometer and diluted to give 50,000 cells per well. Cells were added to 96-well plates containing binding buffer (transport buffer at 0 °C) with appropriate compounds. Final assay volume was 50 μl. Nonspecific binding of [^{3}H]nisoxetine by transfected cells was determined in the presence of 200 μM dopamine. Transfected cells were exposed to [^{3}H]nisoxetine for 60 min at 0 °C. Bound and free radioactivity were separated by rapid vacuum filtration onto GF/B filters (Whatman, Boston, MA) pretreated with 0.6% polyethylenimine. Filters were washed three times with ice-cold phosphate-buffered saline and dried. Filter-retained radioactivity was quantified by liquid scintillation counting. Triplicate measures were made for each experiment ($n = 2–6$ experiments).

Homology Modeling—The FASTA format of the hNET and bLeuT sequences were retrieved and alignments made using the alignments of prokaryotic and eukaryotic Na^+ dependent transporters developed by Beuming *et al.* (21), with additional manual adjustments specific for monoamine transporters (see Fig. 1*B*). The leucine transporter crystal structure (Protein Data Bank code 2A65) was loaded in the INSIGHT II (Accelrys, San Diego, CA) environment and used as a template. Ten homology models of the NET based on our sequence alignment was built on a Silicon Graphics Octane R120000 work station using the MODELLER program (22). N and C termini were not included in the model building process. The most energetically favorable model was chosen for analysis and to produce the figures. The water accessible path (Fig. 6) was calculated using the CAVER program (23) and rendered with PyMOL.

Statistics and Data Analysis—Data are expressed as means ± S.E. (or 95% confidence interval range) of averaged results obtained from 2–8 separate experiments. Either analysis of variance with post hoc *t*-tests performed by the Tukey method or Student's *t* tests were used to evaluate the statistical significance of differences between groups. Values of $p < 0.05$ were

FIGURE 1. *A*, topological map of the NET protein built from the bLeuT (Protein Data Bank code 2A65) (20). Transmembrane helices are shown as stacked residues and are numbered 1–12 in *light blue*. Helical features are based on the homology model of the crystal structure of bLeuT (20). The C and N termini are intracellular and extracellular loops are labeled *dark red*. *Filled circles* indicate the residues mutated in this study. Red filled residues designate residues important for MrIA binding. *B*, sequence alignments of human NET, DAT, SERT, and bLeuT (20) were as described by Beuming *et al.* (21) and manual alignment (*black lines* above sequences). An automated alignment built in Insight II (Accelerys, San Diego, CA) produced a comparable result. Transmembrane helical motifs are highlighted in *light blue* and labeled and additional helical motifs are colored *purple*. Residues highlighted with the same color indicate conserved and partially conserved residues. The *asterisks* indicate the individual residues mutated in this study. The *red underlined region* indicates an EL2 chimera constructed by inserting the corresponding section DAT into NET.

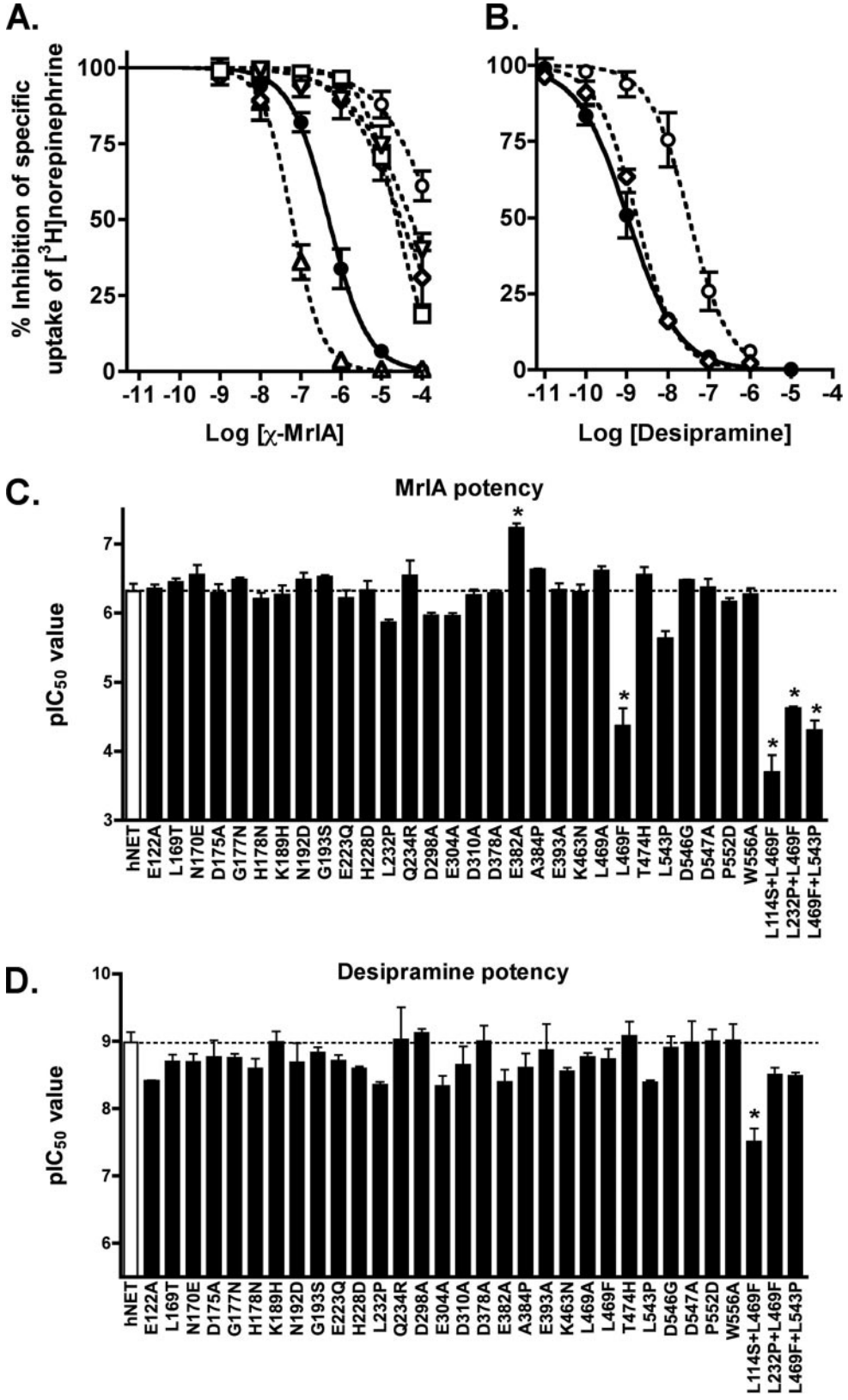

FIGURE 2. **Effect of NET mutants on the IC_{50} of MrIA and desipramine inhibition of [^{3}H]NE uptake.** *A* and *B*, representative concentration-response curves for MrIA (*A*) or DMI at selected mutants (*B*). COS-1 cells transiently transfected with wild-type (● with *solid lines*) or mutant NETs (*dotted lines*) and inhibition of NE uptake for E382A (△), L469F (◇), L114S + L469F (○), L232P + L469F (□), or L469F + L543P (▽) by MrIA or desipramine. Each data set was normalized to transport in the absence of MrIA. Curves were obtained by non-linear regression analyses based on a sigmoidal model. Nonspecific uptake was determined in the presence of desipramine (10^{-4} M) for the wild-type and mutant NETs. *C* and *D*, comparison of pIC_{50} values of mutant NETs determined from inhibition of NE uptake by either MrIA (*C*) or desipramine (*D*). All mutants produced for this study are shown, except where NE uptake was unable to be determined. Values are means ± S.E. of 2–3 separate experiments each performed in triplicate.

considered significant. Curve fitting of saturation binding, transport kinetic and concentration-response data were performed by non-linear regression using Prism 4.0 software (GraphPad, San Diego, CA).

RESULTS

Construction of hNET Mutants—To further investigate the residues involved in MrIA inhibition of NE uptake, mutations of hNET were made by introducing DAT residues into regions of difference. All the mutated NETs (Fig. 1) were confirmed by sequence analysis before transient transfection into COS-1 cells. All NET mutations, except F207T, S225H, H296S, T381K, and D473A, produced uptake of [^{3}H]NE that was not significantly different from uptake by wild-type NET and susceptible to inhibition by desipramine (DMI). Specific uptake for wild-type NET under these experimental conditions was 1.776 ± 0.35 pmol/mg of protein/min (n = 8).

Inhibition of [^{3}H]NE Uptake by MrIA and DMI at Single Point Mutants of hNET—Mutations of hNET that produced readily measurable [^{3}H]NE uptake were assessed for susceptibility to MrIA and desipramine inhibition (Fig. 2). Concentration-response curves for NET mutants affecting IC_{50} of MrIA or DMI are shown in Fig. 2, *A* and *B*, respectively. The pIC_{50} ($-\log IC_{50}$) values for MrIA and DMI at each mutation are shown in Fig. 2, *C* and *D*, respectively. These studies reveal that single residue changes at position 382 (E382A) significantly reduced (8.3-fold) the IC_{50} of MrIA for the NET compared with wild type (Fig. 2*C*) without affecting DMI inhibition. Conversely, a single change at position 469 (L469F) significantly increased (88-fold) the IC_{50} of MrIA for inhibition of the NET (Fig. 2*C*) without affecting DMI inhibition. The reverse mutation of DAT, F472L, conferred MrIA sensitivity which was significant at the mutant but not at the wild type DAT in dopamine uptake assays (mutant pIC_{50} = 3.70 ± 0.13; n = 3). In contrast, the pIC_{50} values for DMI inhibition of [^{3}H]NE uptake were not affected by any of these single point mutations (Fig. 2*D*). In addition, 3.9–4.3-fold increases in IC_{50} approaching significance (p = 0.054 by t test) were observed for both MrIA and DMI at the L232P and L543P mutants (Fig. 2, *C* and *D*), suggesting a potential overlap of MrIA and DMI binding sites on NET.

Double Mutations and Chimera of hNET—Due to the marked effect of L469F on the pIC_{50} value for MrIA, the double mutants L232P + L469F and L469F + L543P of hNET were constructed to determine the extent of any interactions between these positions (Fig. 2). The double mutant L114S + L469F of hNET was also assessed (Fig. 2), since L114S increased MrIA and DMI IC_{50} values ~3-fold (24). All double mutations gave IC_{50} values for MrIA inhibition of [^{3}H]NE uptake that were significantly increased compared with the hNET value (Fig. 2, *A* and *C*) but not significantly different to the single mutant value for L469F, indicating there was no additive effect. L114S + L469F also significantly increased (30-fold) the IC_{50} value of DMI for inhibition of [^{3}H]NE uptake (Fig. 2*D*). The other double mutants L232P + L469F and L469F + L543P

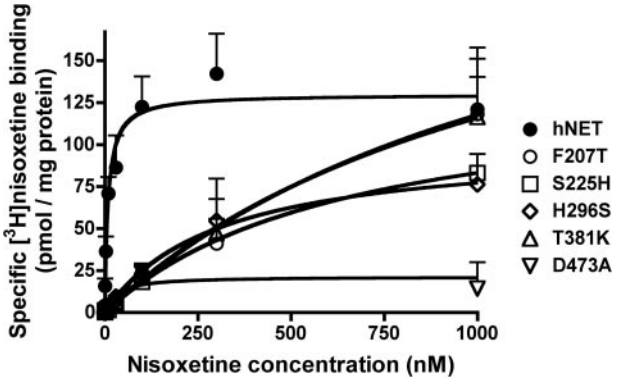

FIGURE 3. **Saturation binding of [^{3}H]nisoxetine at hNET and mutants showing poor [^{3}H]NE uptake.** COS-1 cells transiently transfected with hNET (●) or mutant NETs; F207T (○), S225H (□), H296S (◇), T381K (△), or D473A (▽) were incubated for 60 min at 0 °C with increasing concentrations of [^{3}H]nisoxetine. Each point is the mean ± 95% confidence interval determined from 3–6 experiments each performed in triplicate. The curves were obtained by non-linear regression analyses according to a hyperbolic model. Specific binding was calculated as the difference between binding in the absence and presence of 200 μM dopamine.

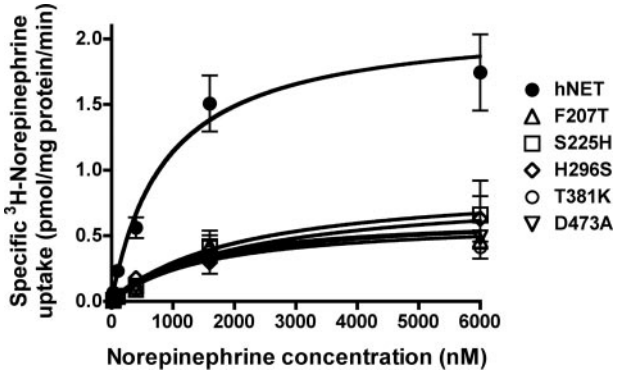

FIGURE 4. **Saturation of [^{3}H]NE uptake by mutants with poor [^{3}H]NE uptake.** COS-1 cells transiently transfected with hNET (●) or mutant NETs F207T (△), S225H (□), H296S (◇), T381K (○), or D473A (▽) were incubated for 5 min at room temperature with increasing concentrations of [^{3}H]NE. Each point is the mean ± 95% confidence interval determined from three to six experiments each performed in triplicate. The curves were obtained by non-linear regression analyses according to a hyperbolic model. Specific uptake was calculated as the difference between uptake in the absence and presence of 100 μM nisoxetine.

TABLE 1
[^{3}H]NE transport and [^{3}H]nisoxetine binding at hNET and selected mutants

	[^{3}H]NE, K_m	Normalized [^{3}H]NE, V_{max}	[^{3}H]Nisoxetine K_d	Normalized [^{3}H]nisoxetine, B_{max}
	nM		nM	
hNET[a]	690 (320, 1490)[b]	1.0	5.1 (2.3, 11)[b]	1.0
F207T	720 (260, 1930)	0.26 (0.1, 0.7)[c]	319 (81, 1260)[c]	0.60 (0.1, 2.6)
S225H	1870 (157, 6966)	0.31 (0.1, 0.9)[c]	656 (194, 1120)[c]	1.1 (0.6, 1.5)
H296S	1190 (200, 7160)	0.25 (0.1, 0.6)[c]	257 (62, 1070)[c]	0.66 (0.3, 1.4)
T381K	530 (190, 1480)	0.17 (0.1, 0.3)[c]	650 (156, 2720)[c]	0.82 (0.3, 2.5)
D473A	1580 (400, 6280)	0.26 (0.1, 0.5)[c]	47 (17, 130)[c]	0.19 (0.1, 0.7)[a]

[a] V_{max} for hNET = 1.776 ± 0.35 pmol/mg of protein/min; B_{max} for hNET = 129.5 ± 14.5 pmol/mg of protein (n = 8 experiments).
[b] 95% confidence interval values shown in parentheses (n = 3–8 experiments).
[c] Significantly different from wild-type hNET.

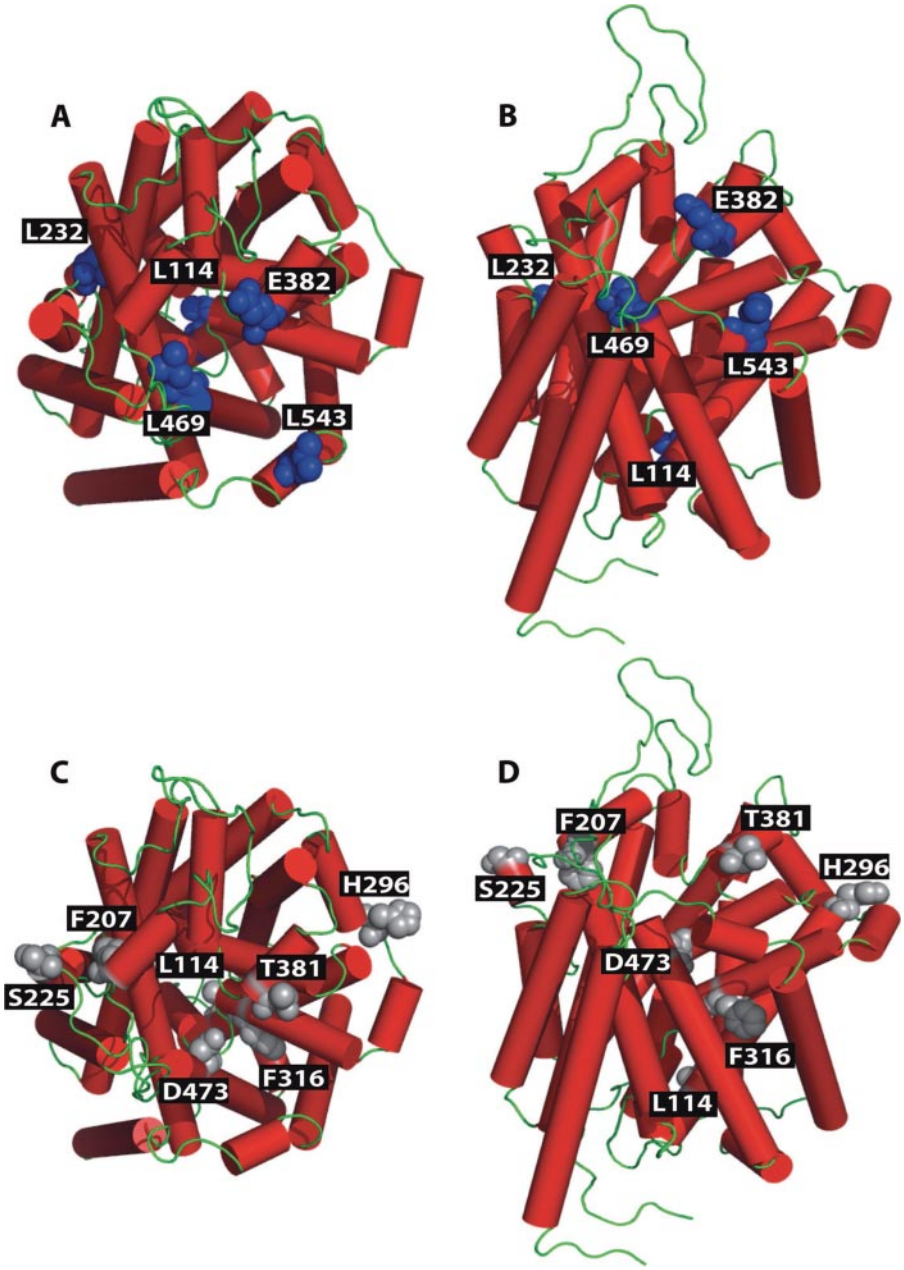

FIGURE 5. **Homology model of the NET protein constructed from the crystal structure of the Na^+-dependent bLeuT (20).** Helical structures are shown in red. Top (*A*) and side (*B*) views of NET showing residues that affected MrIA affinity (Leu^{114} (24), Leu^{232}, Glu^{382}, Leu^{469}, and Leu^{543} in *blue*). Top (*C*) and side (*D*) views of NET showing residues that affected [^{3}H]nisoxetine affinity (Leu^{114} (24), Phe^{207}, Ser^{225}, His^{296}, Phe^{316} (28), Thr^{381}, and Asp^{473} in *gray*). Leu^{469} also reduced the affinity of [^{3}H]nisoxetine as the double mutant with Leu^{114}.

caused small increases (~3-fold, which was not significant) in the IC_{50} value of DMI (Fig. 2*D*), similar to the increase seen previously for L114S alone (24). The EL2 chimera did not significantly affect the ability of DMI (pIC_{50} 9.13 ± 0.12) or MrIA (pIC_{50} 6.8 ± 0.12) to inhibit NE uptake in this mutant.

hNET Mutants with Poor Specific Uptake of [^{3}H]NE—In our initial studies, the F207T, S225H, H296S, T381K, and D473A mutants of hNET failed to show significant [^{3}H]NE uptake. Lack of apparent [^{3}H]NE uptake could arise from (i) a marked reduction in cell surface expression of protein (for example as a result of protein misfolding), (ii) a marked reduction in the affinity of NE for the transporter, and/or (iii) effects on the translocation or gating mechanism of NET. To establish if NET expression was affected, we determined the B_{max} and K_d for [^{3}H]nisoxetine binding to these mutants (Fig. 3). B_{max} (maximal binding) has been shown previously to provide a good measure of surface expression (25). Using a similar approach, F207T, T381K, S225H, and H296S produced maximal binding that was not significantly different to wild-type hNET, while D473A produced ~20% wild-type binding (Fig. 3 and Table 1). F207T, T381K, S225H, and H296S also significantly increased (30–130-fold) the K_d for [^{3}H]nisoxetine compared with hNET, while the D473A mutant produced a 9-fold increase in K_d (Table 1). Since specific [^{3}H]nisoxetine binding was detectable for all mutants, we reassessed their ability to transport [^{3}H]NE using higher NE substrate concentrations (Fig. 4). Under these conditions, all mutants displayed measurable uptake of [^{3}H]NE (Fig. 4), with maximal uptake reduced 3–6-fold compared with hNET (Table 1 and Fig. 4). The K_m of NE for these mutants was not significantly altered despite the K_d of [^{3}H]nisoxetine being dramatically affected (Table 1, Fig. 4). Unfortunately, assays measuring specific [^{3}H]NE uptake or specific [^{3}H]nisoxetine binding had poor signal to noise and we were unable to measure the IC_{50} of MrIA at these mutants using these assays.

Homology Model of the hNET—A homology model of the hNET was constructed using bLeuT as a template (Fig. 5). The structure maintains 12 membrane spanning helices (TM) as previously predicted by hydrophobicity analysis (12). As defined by bLeuT, the majority of the helices are not perpendicular to the lipid bilayer but angled to form a pore with a wide external mouth and associated gating structure (including elements from EL2 and EL4). This architecture uses helices of widely varying lengths (Figs. 1*A* and 5) including several amphipathic helices (TM3, TM8, and TM10) exposed on the extracellular surface and potentially lying along the top of the lipid bilayer (extracellular loops EL3 and EL6) and helices potentially lining a water-filled translocation pathway (TM1 and TM6) (Fig. 5). Amino acid residues influencing the affinity of the

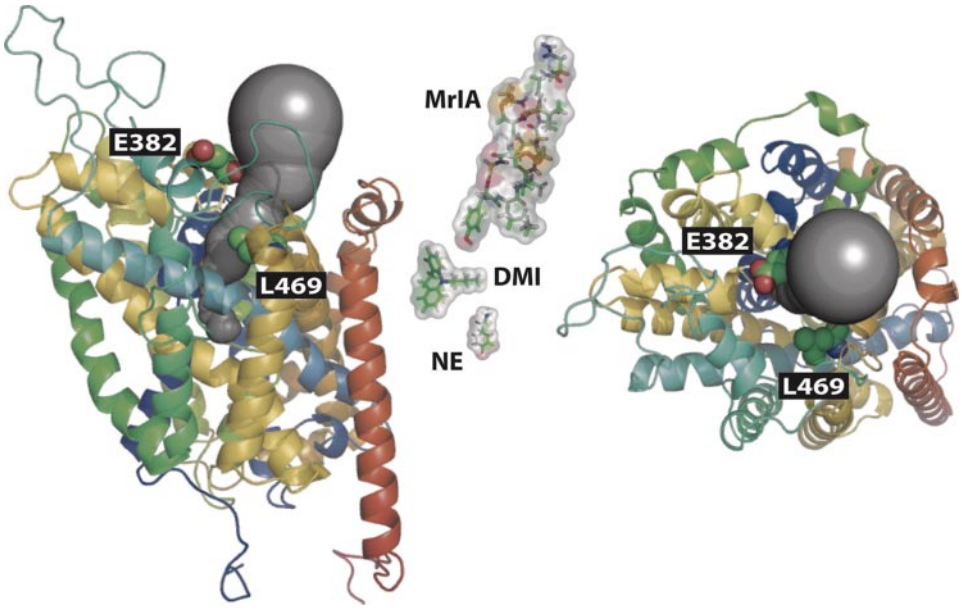

FIGURE 6. **Proposed binding positions of MrIA, the tricyclic DMI, and NE at NET.** The homology model of human NET in ribbon representation (from Fig. 5) shows the presumed water-filled pathway (*gray* volume) linking the extracellular space to the substrate binding site (calculated using CAVER (23)). Residues with largest effect on MrIA binding (Glu^{382} and Leu^{469}) are shown in Corey-Pauling-Koltun representation. MrIA, DMI, and NE are shown in *stick* and transparent molecular surface rendition at the same scale as NET. Vertical positions of MrIA, DMI, and NE in the pore of NET are shown relative to the side view of NET (*left panel*). *Right panel* shows the top (90° rotated) view of *left panel*. Overlap apparent between MrIA/DMI and DMI/NE but not MrIA/NE is consistent with the competitive MrIA/DMI and DMI/NE interactions and the noncompetitive MrIA/NE interaction (11).

transporter for MrIA (Fig. 5, *A* and *B*) and nisoxetine (Fig. 5, *C* and *D*) are highlighted.

DISCUSSION

Using site-directed mutagenesis to introduce DAT residues into human NET (Fig. 1), we have identified new positions affecting χ-MrIA (L469F) and tricyclic antidepressant (F207T, T381K, S225H, and H296S) binding to NET. An additional eight NET mutants with negatively charged residues predicted to lie in extracellular loops replaced with alanine also identified a potential MrIA clash (E382A) and an additional contributor to tricyclic binding (D473A). To start to understand how these mutants affected inhibitor interactions with NET, we constructed a homology model of NET (Figs. 5 and 6) from the bLeuT structure, the closest related Na^+-dependent transporter crystallised (20). Examination of this model revealed that most of the interacting residues identified in this study clustered near the predicted entrance for NE transport (Fig. 5), providing experimental support for the bLeuT-derived model of NET.

Of the 33 positions examined, E382A enhanced (8-fold) and L469F reduced (88-fold) the affinity of MrIA to inhibit NE uptake by hNET. Given the predicted position of Glu^{382} in the mouth of NET (Figs. 5*A* and 6), its charge and/or size might possibly hinder MrIA binding. In a previous alanine scan of MrIA, four residues (Tyr^7, Lys^8, Leu^9, and His^{11}) were identified as contributing directly to MrIA inhibition of NET transport (11). Given the negative effect of Glu^{382} on MrIA binding and the lack of effect of replacing other negative charges in the extracellular loops, potential salt bridges between NET residues and the Lys^8 or His^{11} of MrIA do not appear to contribute to affinity. Leu^{469} is situated at the mouth of NET in close proximity to Glu^{382} (C^α–C^α distance: ~15 Å). However, in this instance replacing it with the corresponding DAT residue (Phe) markedly reduced the affinity of MrIA to inhibit NE uptake. Likewise, changing Phe^{472} of DAT to the NET residue leucine made the DAT sensitive to MrIA inhibition, confirming that this residue has an important influence on MrIA affinity. Since the L469A mutant had no effect on MrIA inhibition, it appears that smaller hydrophobic residues at this position support high affinity MrIA binding and that the hydrophobic and bulky Phe interferes with MrIA binding, presumably due to a steric clash. The small increases in IC_{50} of MrIA at the L232P and L543P mutants, which approached significance in these studies, may arise from structural perturbations associated with the introduction of Pro (26, 27). According to the homology model, these residues are in external loops on opposite sides of NET where they could influence the conformation of the mouth of NET. Double mutants of these residues together with L469F did not have any additional impact on MrIA affinity, indicating that any effect of these residues was relatively minor. In a previous study, residue L114A and L114S mutants reduced MrIA, antidepressant (desipramine) and cocaine affinity to similar extents (3–10-fold) (24). In the present study, the L469F + L114S double mutant did not show any additive effects on MrIA IC_{50}.

In contrast to MrIA, none of the single point mutations of hNET described above affected desipramine IC_{50}. However, the L469F + L114S double mutant caused a 32-fold increase in desipramine IC_{50}, 5-fold greater than seen for the single L114S mutation alone (24). After examination of the homology model, it is apparent that L114 is positioned intracellularly, where it is unlikely to have any direct interaction with either substrates or inhibitors. Hence it is most likely that the L114S mutation introduces a structural change or conformational shift in NET, as suspected from its similar effect on IC_{50} across a range of unrelated inhibitors (24). Apparently, this mutation exposes an otherwise silent effect of L469F, to further increase the IC_{50} for desipramine. The chimera of extracellular loop 2 of DAT and NET had no effect on DMI or MrIA inhibition of NE uptake and is unlikely to be involved in the binding of either inhibitor.

Of the hNET mutants constructed, F207T, S225H, H296S, and T381K showed poor NE uptake despite normal nisoxetine B_{max} values, indicating that the rate of NE transport was diminished while surface expression remained unchanged (NET turnover (V_{max}(NE)/B_{max}(nisoxetine)) was reduced 2.3–5-fold). The other poor transporter D473A had a

5-fold reduced B_{max}, indicating expression levels for this mutant were reduced (24), accounting for the reduced NE transport observed. While these mutants had no effect on K_m value of NE, they had a dramatic effect on nisoxetine K_d. Mutations affecting transport rate (F207T, T381K, S225H, and H296S) caused a 30–130-fold reduction in [^{3}H]nisoxetine affinity, while the D473A mutant caused a smaller (9-fold) reduction. Examining the homology model revealed that all residues affecting NE transport and nisoxetine affinity were located at the ends of extracellular helices that either lined (Thr^{381} and Asp^{473}) or were just outside (Phe^{207}, Ser^{225}, and His^{296}) the mouth of the transporter. While residues lining the mouth of NET could directly influence both affinity and transport, mutations outside the mouth might be expected to indirectly reduce affinity and transport by disrupting the structure and/or gating of NET. Unfortunately, we were unable to assess the IC_{50} of MrIA at these mutants. Earlier studies identified two mutations that caused 6-fold shifts in the IC_{50} of DMI to inhibit NE uptake (28), Phe^{316}, which appears near the center of the transporter, and Leu^{114}, which is located intracellularly (Fig. 5).

Previous models of the dopamine and serotonin transporters (15, 17, 29, 30) were based on functionally unrelated transporters such as the sodium hydrogen antiporter (NhaA transporter) (31), glutamate (16), and Lac permease (32) transporters. While these models incorporated mutagenesis and biochemical data, the templates had low homology (~12%) and limited functional similarity. In contrast, hNET and bLeuT have 28% sequence homology and both are Na^+-dependent transporters and thus expected to share secondary, tertiary, and quaternary structure. A similar level of homology between the functionally related nicotinic acetylcholine receptor and the molluscan acetylcholine-binding protein allows the production of predictive homology models of the nicotinic acetylcholine receptor (33). The new model of NET shows a tapered water-filled cavity that restricts intracellular access and several external helical loops positioned around the mouth of the pore that could influence ligand binding (Fig. 6). The deepest portion of this cavity allows the binding of NE at the same location as the leucine seen in bLeuT. Consistent with results of our previous studies (11), the model allows partially overlapping MrIA/tricyclic binding and tricyclic/NE binding but discrete MrIA/NE binding. It is also consistent with previous NET mutant data (6, 28, 34). This model should prove useful in guiding the design of improved inhibitors of NET.

Acknowledgments—MrIA was a gift from Xenome Ltd. The homology model Protein Data Bank file can be found at the Institute for Molecular Bioscience website (group leader, Lewis, links, atomic coordinates).

REFERENCES

1. Torres, G. E., Gainetdinov, R. R., and Caron, M. G. (2003) *Nat. Rev. Neurosci.* **4,** 13–25
2. Stahl, S. M. (2003) *J. Clin. Psychiatry* **64,** 230–231
3. Gainetdinov, R. R., and Caron, M. G. (2003) *Annu. Rev. Pharmacol. Toxicol.* **43,** 261–284
4. Schroeter, S., Apparsundaram, S., Wiley, R. G., Miner, L. H., Sesack, S. R., and Blakely, R. D. (2000) *J. Comp. Neurol.* **420,** 211–232
5. Nielsen, C. K., Lewis, R. J., Alewood, D., Drinkwater, R., Palant, E., Patterson, M., Yaksh, T. L., McCumber, D., and Smith, M. T. (2005) *Pain* **118,** 112–124
6. Paczkowski, F. A., and Bryan-Lluka, L. J. (2001) *Brain Res. Mol. Brain Res.* **97,** 32–42
7. Paczkowski, F. A., and Bryan-Lluka, L. J. (2004) *J. Neurochem* **88,** 203–211
8. Bonisch, H., Runkel, F., Roubert, C., Giros, B., and Bruss, M. (1999) *J. Auton Pharmacol.* **19,** 327–333
9. Sucic, S., and Bryan-Lluka, L. J. (2002) *Brain Res. Mol. Brain Res.* **108,** 40–50
10. Sharpe, I. A., Gehrmann, J., Loughnan, M. L., Thomas, L., Adams, D. A., Atkins, A., Palant, E., Craik, D. J., Adams, D. J., Alewood, P. F., and Lewis, R. J. (2001) *Nat. Neurosci.* **4,** 902–907
11. Sharpe, I. A., Palant, E., Schroeder, C. I., Kaye, D. M., Adams, D. J., Alewood, P. F., and Lewis, R. J. (2003) *J. Biol. Chem.* **278,** 40317–40323
12. Pacholczyk, T., Blakely, R. D., and Amara, S. G. (1991) *Nature* **350,** 350–354
13. Norregaard, L., and Gether, U. (2001) *Curr. Opin. Drug Discovery Dev.* **4,** 591–601
14. Appell, M., Berfield, J. L., Wang, L. C., Dunn, W. J., 3rd, Chen, N., and Reith, M. E. (2004) *Biochem. Pharmacol.* **67,** 293–302
15. Ravna, A. W., Sylte, I., and Dahl, S. G. (2003) *J. Comput. Aided Mol. Des.* **17,** 367–382
16. Yernool, D., Boudker, O., Jin, Y., and Gouaux, E. (2004) *Nature* **431,** 811–818
17. Ravna, A. W., and Edvardsen, O. (2001) *J. Mol. Graph. Model.* **20,** 133–144
18. Rasmussen, S. G. F., Adkins, E. M., Carroll, F. I., Maresch, M. J., and Gether, U. (2003) *Eur. J. Pharmacol.* **479,** 13–22
19. Sen, N., Shi, L., Beuming, T., Weinstein, H., and Javitch, J. A. (2005) *Neuropharmacology* **49,** 780–790
20. Yamashita, A., Singh, S. K., Kawate, T., Jin, Y., and Gouaux, E. (2005) *Nature* **437,** 215–223
21. Beuming, T., Shi, L., Javitch, J. A., and Weinstein, H. (2006) *Mol. Pharmacol.* **70,** 1630–1642
22. Sali, A., and Blundell, T. L. (1993) *J. Mol. Biol.* **234,** 779–815
23. Petrek, M., Otyepka, M., Banas, P., Kosinova, P., Koca, J., and Damborsky, J. (2006) *BMC Bioinformatics* **7,** 316
24. Bryan-Lluka, L. J., Bonisch, H., and Lewis, R. J. (2003) *J. Biol. Chem.* **278,** 40324–40329
25. Apparsundaram, S., Galli, A., DeFelice, L. J., Hartzell, H. C., and Blakely, R. D. (1998) *J. Pharmacol. Exp. Ther.* **287,** 733–743
26. Barlow, D. J., and Thornton, J. M. (1988) *J. Mol. Biol.* **201,** 601–619
27. Sansom, M. S., and Weinstein, H. (2000) *Trends Pharmacol. Sci.* **21,** 445–451
28. Roubert, C., Cox, P. J., Bruss, M., Hamon, M., Bonisch, H., and Giros, B. (2001) *J. Biol. Chem.* **276,** 8254–8260
29. Edvardsen, O., and Dahl, S. G. (1994) *Brain Res. Mol. Brain Res.* **27,** 265–274
30. Ravna, A. W., Sylte, I., and Dahl, S. G. (2003) *J. Pharmacol. Exp. Ther.* **307,** 34–41
31. Williams, K. A. (2000) *Nature* **403,** 112–115
32. Abramson, J., Smirnova, I., Kasho, V., Verner, G., Kaback, H. R., and Iwata, S. (2003) *Science* **301,** 610–615
33. Dutertre, S., and Lewis, R. J. (2004) *Eur. J. Biochem.* **271,** 2327–2334
34. Sucic, S., Paczkowski, F. A., Runkel, F., Bonisch, H., and Bryan-Lluka, L. J. (2002) *J. Neurochem.* **81,** 344–354